View Article Online
DOI: 10.1039/D0CP02094J

PEM fuel cell distribution of relaxation times: A method for calculation and behavior of oxygen transport peak

Andrei Kulikovsky[1, a)]
Forschungszentrum Jülich GmbH
Institute of Energy and Climate Research,
IEK–14: Electrochemical Process Engineering
D–52425 Jülich, Germany [b)]

(Dated: 29 July 2020)

A simple numerical method for calculation of the distribution of relaxation times (DRT) for PEM fuel cell impedance is developed. The method combines Tikhonov regularization technique and projected gradient iterations. The method is illustrated by calculating DRT for synthetic impedance of two parallel RC–circuits and of Warburg finite–length impedance. Finally, cathode catalyst layer (CCL) impedance is calculated using exact analytical solution and the method discussed is applied to understand behavior of DRT peak due to oxygen transport in the CCL. Position of the oxygen transport peak on the frequency scale exhibits non–monotonic behavior as the oxygen diffusion coefficient in the CCL decreases, which may serve as indicator of CCL flooding. The Python code for DRT calculation is available for download.

Keywords: PEM fuel cell; Distribution of relaxation times; modeling

I. INTRODUCTION

Electrochemical impedance spectroscopy (EIS) is a powerful tool for understanding fundamental processes in a fuel cell[1,2]. While polarization curve gives the total potential loss in the cell, EIS makes it possible to separate contributions of different processes into this loss and to calculate the basic transport and kinetic parameters of the cell[3]. This explains tremendous interest in EIS from the fuel cell community: in recent years, a number of publications on fuel cell impedance has been growing exponentially.

Understanding impedance spectra is, however, nontrivial task. Basically, there are two options for processing experimental spectra. A standard approach implies heuristic construction of equivalent circuit and fitting the circuit elements to the experimental spectrum of a fuel cell. In this way, basic cell resistivities and capacitance can be obtained (see e.g.[4–7]). However, a much more informative and reliable approach is physical impedance modeling (see e.g.,[8–16]).

An alternative and complementary technique for impedance spectra analysis is Distribution of Relaxation Times (DRT)[17–22]. In its present form, this technique has been suggested in 1941 by Fuoss and Kirkwood[23] and brought to the fuel cell community seemingly by Schlichlein et al.[17]. An introduction to DRT analysis and history of DRT research has recently been given by Ivers–Tiffée and Weber[24].

The idea of DRT technique is as following. Let the fuel cell impedance be $Z(\omega)$; DRT function $\gamma(\tau)$ is a solution

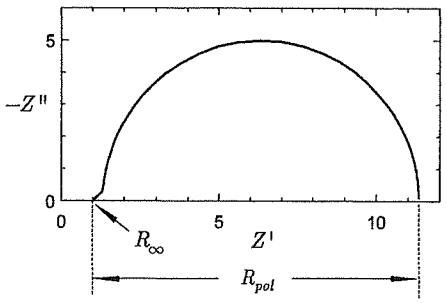

FIG. 1. Schematic of a typical Nyquist spectrum of PEM fuel cell.

to equation

$$Z(\omega) - R_\infty \quad R_{pol} \int_0^\infty \frac{\gamma(\tau)\, d\tau}{1 + i\omega\tau} \tag{1}$$

Here $R_\infty \equiv Z|_{\omega\to\infty}$ is the high–frequency (ohmic) cell resistance, and $R_{pol} = Z|_{\omega\to 0} - R_\infty$ is the total polarization resistance of a fuel cell (Figure 1). Setting in Eq.(1) $\omega = 0$, we see that γ obeys the normalization condition

$$\int_0^\infty \gamma(\tau)\, d\tau \quad 1 \tag{2}$$

Eq.(1) stems from the following idea. Impedance of a parallel RC–circuit is

$$Z_{RC} = \frac{R}{1 + i\omega RC} \tag{3}$$

Denoting here $RC = \tau$ and integrating the right side over τ with the weight function $\gamma(\tau)$, we get the right side of Eq.(1). Thus, Eq.(1) can be considered as expansion of

a)Electronic mail: A.Kulikovsky@fz-juelich.de
b)Also at:Lomonosov Moscow State University, Research Computing Center, 119991 Moscow, Russia

View Article Online
DOI: 10.1039/D0CP02094J 2

fuel cell impedance over infinite sum of parallel RC–circuits, each one having the resistance of $R_{pol}\gamma\, d\tau$.

Suppose now that impedance Z corresponds to the parallel RC–circuit. Setting in Eq.(1) $Z \quad Z_{RC}$, $R_{pol} \quad R$ and $R_\infty = 0$, we see that solution to Eq.(1) is the Dirac delta–function $\gamma(\tau) = \delta(\tau - RC)$. This result shows that for every RC–like arc in the Nyquist spectrum, the DRT function $\gamma(\tau - \tau_*)$ contains a δ function–like peak at τ_*, with τ_* being the characteristic time constant of the process.

In the frequency range below the summit frequency of faradaic arc, the faradaic impedance of a PEM fuel cell is close to impedance of RC–circuit[25]. Thus, we may expect that the DRT peak corresponding to the faradaic arc of a fuel cell is close in shape to δ–function. However, huge gradient of a δ–like function poses specific problems in numerical calculation of γ.

To illustrate this effect, we separate the real Z' and imaginary Z'' parts of Eq.(1)

$$Z'(\omega) \quad R_\infty + R_{pol}\int_0^\infty \frac{\gamma(\tau)\, d\tau}{1+\omega^2\tau^2} \tag{4}$$

$$Z''(\omega) = -R_{pol}\int_0^\infty \frac{\omega\tau\gamma(\tau)\, d\tau}{1+\omega^2\tau^2} \tag{5}$$

In view of Kramers–Kronig relations, any of Eqs.(4), (5) can be used for calculation of γ. Eqs.(4), (5) belong to the class of Fredholm equations of the first kind. It is well known, that any direct numerical approximation of Eqs.(4), (5) leads to an ill–posed problem. Consider for definiteness Eq.(5); straightforward approach to numerical solution of this equation implies approximation of the right side by some numerical integration formula on a discrete mesh $\{\tau_n; n = 1,\ldots,N\}$. Using the simplest integration scheme, we get

$$Z''(\omega_m) = -R_{pol}\sum_{n=1}^{N} \frac{\omega_m\tau_n\gamma_n\,\delta\tau_n}{1+\omega_m^2\tau_n^2} \tag{6}$$

where $\gamma_n \equiv \gamma(\tau_n)$, $\tau_n = 1/\omega_n$, and $\delta\tau_n = \tau_{n+1} - \tau_n$. In the matrix notations, Eq.(6) has the form

$$\mathbf{A}\vec{\gamma} = \vec{Z}'', \quad \text{with} \quad A_{m,n} = -R_{pol}\frac{\omega_m\tau_n\delta\tau_n}{1+\omega_m^2\tau_n^2} \tag{7}$$

The system of linear equations (7) is ill–posed and to solve it Tikhonov regularization (TR) technique[26] has to be used. In its simplest form, the TR algorithm for this system reads

$$\left(\mathbf{A}^T\mathbf{A} + \lambda\mathbf{I}\right)\vec{\gamma} = \mathbf{A}^T\vec{Z}'' \tag{8}$$

where $\mathbf{I}$ is the identity matrix, $\mathbf{A}^T$ means transposed matrix $\mathbf{A}$ and λ is the regularization parameter. Unfortunately, even with the proper regularization parameter, numerical solution to Eq.(8) does not guarantee positiveness of γ. This effect is illustrated in Figure 2, where the solution to Eq.(8) for $Z''(\omega)$ corresponding to the parallel RC–circuit with $R = C = 1$ is plotted. Though the main peak of γ is located at the point $\tau_* = 1$ corresponding to the characteristic time constant of the RC–circuit, large non–physical

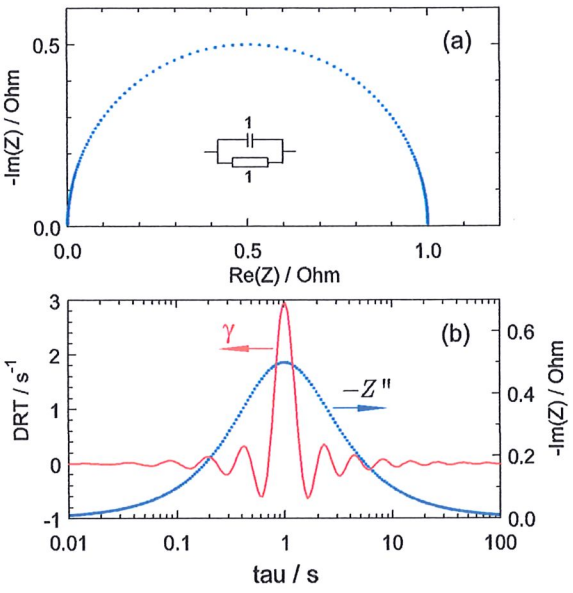

FIG. 2. (a) Nyquist plot of impedance of a single parallel RC–circuit with $R = C = 1$. (b) solid line – DRT for impedance in (a) obtained by direct Tikhonov regularization solution to Eq.(6); points – imaginary part of impedance in (a).

oscillations of $\gamma(\tau)$ are clearly seen. Obviously, these oscillations result from large gradients of the exact solution to Eq.(5), which in this case is $\delta(\tau - 1)$.

The problem of numerical solution of Eq.(1) under the constrain $\gamma \geq 0$ has been discussed in fuel cell and battery literature and a number of iterative algorithms penalizing negative solutions have been developed[20,27–30]. The cost of "forcing" the solution of Eq.(7) to be positive is a significant complication of the solution methods, as compared to standard Tikhonov regularization, Eq.(8). In addition, proper choice of regularization parameter(s) is a non–trivial task: the shape and even the number of peaks in the numerical $\gamma(\tau)$ distribution depend on this choice, which retards identification of the physical processes[31]. Alternative approaches to DRT calculation include Fourier transform of Eq.(1)[32], and genetic algorithms finding a best–fit system of probe functions for DRT[18,33]. However, in domains of large DRT gradients, Fourier transform method leads to non–physical negative oscillations, while evolutionary codes are accurate, but rather slow.

In this work, we report a simple and fast method for calculation of DRT for PEM fuel cell impedance. The method combines the Tikhonov regularization technique with the projected gradient (PG) iterations (TRPG–method). A key feature of the method is that the two regularization parameters λ_T and λ_{pg} appearing in the TRPG–iteration scheme are obtained using least–squares minimization of the Tikhonov residual. From the user's perspective, it means

View Article Online
DOI: 10.1039/D0CP02094J 3

that only a reasonable initial guess for λ_T and λ_{pg} has to be set to initiate the solution process; the final optimal values of λ_T and λ_{pg} are sought by the algorithm.

The method is illustrated by calculating DRT for the synthetic impedance of two series–connected parallel RC–circuits and for the Warburg finite–length impedance. Last not least, DRT for analytical cathode catalyst layer (CCL) impedance is calculated and behavior of the oxygen transport peak as a function of oxygen diffision coefficient in the CCL is demonstrated.

II. METHOD

As noted in the Introduction, DRT can be calculated using either real, or imaginary part of impedance; below, $\mathrm{Im}\,(Z)$ will be used. Looking at the direct Tikhonov solution $\vec{\gamma}_T$ in Figure 1b we note that despite of negative oscillations, $\vec{\gamma}_T$ correctly captures position of the main DRT peak. Thus, we can try to "improve" $\vec{\gamma}_T$ by using it as initial guess for the projected gradient (PG) iterations[34]. Further, we will require that PG–iterations minimize the Tikhonov residual, as discussed below.

Specifically, we set $\gamma^0 \quad \gamma_T$ and seek for the parameter vector $(\lambda_T, \lambda_{pg})$ minimizing in the least–squares sense the Tikhonov residual

$$\left(\mathbf{A}^T\mathbf{A} + \lambda_T\mathbf{I}\right)\vec{\gamma}^K - \mathbf{A}^T\vec{Z}'' \to \min, \tag{9}$$

where $\vec{\gamma}^K$ is calculated using K steps of the projected gradient scheme:

$$\vec{\gamma}^{k+1} = \vec{\gamma}^k - \lambda_{pg}\left(\left(\mathbf{A}^T\mathbf{A} + \lambda_T\mathbf{I}\right)\vec{\gamma}^k - \mathbf{A}^T\vec{Z}''\right) \tag{10}$$

$$\gamma_n^{k+1} = \begin{cases} \gamma_n^{k+1}, & \text{if } \gamma_n^{k+1} \geq 0 \\ 0, & \text{otherwise} \end{cases}, \quad n = 1, 2, \ldots, N \tag{11}$$

$$k = 0, 1, \ldots, K-1$$

Here, the matrix $\mathbf{A}$ is calculated according to Eq.(7). The procedure (9)–(11) is repeated until the convergence condition for (9) is achieved.

If the real part of impedance is used for DRT calculations, $\vec{Z}''$ in Eq.(9) should be replaced by $\vec{Z}' - R_\infty$, and the matrix $\mathbf{A}$ should be calculated as

$$A_{m,n} = R_{pol}\frac{\delta\tau_n}{1 + \omega_m^2\tau_n^2} \tag{12}$$

An initial guess for λ_T can be found by the L–curve method (see below). Initial value of the projected gradient parameter λ_{pg} can be found using the following arguments. Eq.(10) can be rewritten in the form

$$\gamma^{k+1} \quad \left\{\mathbf{I} - \lambda_{pg}\left(\mathbf{A}^T\mathbf{A} + \lambda_T\mathbf{I}\right)\right\}\gamma^k + \lambda_{pg}\mathbf{A}^T\vec{Z}'' \tag{13}$$

The norm of the matrix in figure brackets on the right side must be less than unity, otherwise in the course of iterations the norm of $\vec{\gamma}^{k+1}$ would grow. Thus, the following condition must hold:

$$\left\|\mathbf{I} - \lambda_{pg}\left(\mathbf{A}^T\mathbf{A} + \lambda_T\mathbf{I}\right)\right\| < 1 \tag{14}$$

Equating the left side of this equation to zero, by the order of magnitude we have

$$\lambda_{pg} \simeq \frac{1}{\|\mathbf{A}^T\mathbf{A} + \lambda_T\mathbf{I}\|} \tag{15}$$

The code implementing the algorithm above has been written in Python. Eq.(9) is minimized using the *least_squares* module with constrained optimization option *trf* from the SciPy library. Optionally, Levenberg–Marquardt (LM) algorithm of minimization can be invoked; however, being unconstrained, the LM–method may return negative regularization parameters. PG–iterations (10), (11) are stopped when the relative change of the norm $\|\vec{\gamma}\|$ between two successive iterations is less than 10^{-6}. On each iteration step for Eq.(9), the latter condition requires a number of PG–iterations K between 10^3 and 10^5. The code is fast: typically, it takes one to ten seconds to calculate a single DRT spectrum on a 2.4-GHz PC. The time of calculation strongly depends on the initial guess for parameters λ_T and λ_{pg} (see discussion in the next section). A somewhat faster variant of the method is described in Appendix. The code is available for download at
https://github.com/akulikovsky/DRT-python-code .

III. RESULTS AND DISCUSSION

The time scale τ (seconds) is related to the frequency scale as $f = 1/(2\pi\tau)$ (Hz). It is convenient to plot $\gamma(f)$ rather than $\gamma(\tau)$, since peak positions of the spectrum $\gamma(f)$ give characteristic frequencies of physical The tests in this section have been performed using either imaginary, or real part of impedance for DRT calculation, with the following modification in the expressions for the matrix A_{mn} in Eqs.(7), (12): $\delta\tau_n = 0.5(\tau_{n+1} - \tau_{n-1})$ at the internal mesh points and $\delta\tau_0 = 0.5(\tau_1 - \tau_0)$, $\delta\tau_{N-1} = 0.5(\tau_{N-1} - \tau_{N-2})$ at the boundaries. This provides more accurate approximation of integrals in Eqs.(4), (5).

A. Test synthetic impedances

The first test of the method is DRT of impedance of two parallel RC–circuits connected in series. The impedance of the system

$$Z = \frac{R_1}{1 + \mathrm{i}\omega R_1 C_1} + \frac{R_2}{1 + \mathrm{i}\omega R_2 C_2} \tag{16}$$

has been generated on the exponential (uniform on the log-scale) grid with 22 points per decade. Figure 3a shows DRT of this system calculated using the direct Tikhonov regularization technique, Eq.(8). Again, negative oscillations are seen, though the positions of main peaks are captured cor-

View Article Online
DOI: 10.1039/D0CP02094J 4

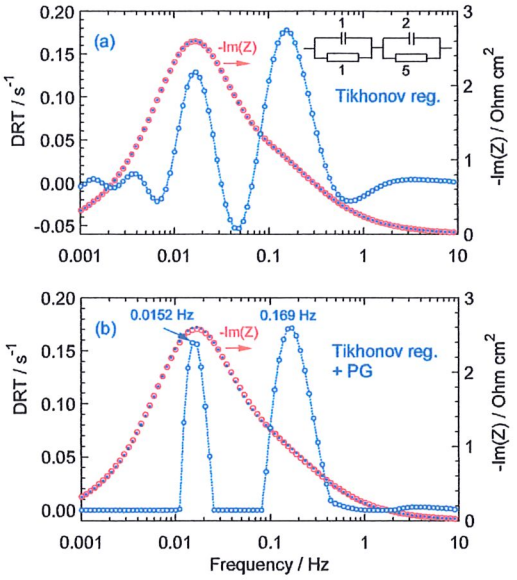

FIG. 3. (a) Tikhonov solution of Eq.(8) for the DRT of two series–connected parallel RC–circuits (connected blue open circles). Solid blue points – imaginary part of exact impedance, Eq.(16), open red circles show $-\mathrm{Im}\,(Z)$ reconstructed from the Tikhnonov's DRT. Solid blue points and open circles are practically indistinguishable. (b) TRPG solution for DRT, Eqs.(9)–(11) and the exact and reconstructed imaginary parts of impedance.

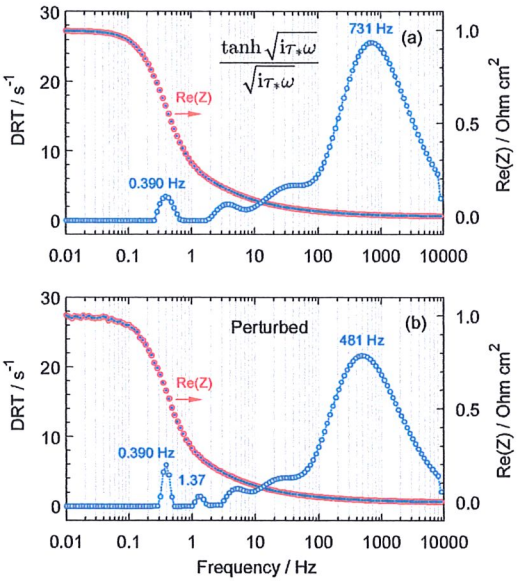

FIG. 4. (a) DRT of Warburg finite–length impedance, Eq.(17), calculated using the TRPG–scheme (connected blue open circles). Solid blue points depict real part of exact impedance, Eq.(17), open red circles show $\mathrm{Re}\,(Z)$ reconstructed from the DRT. (b) The same data calculated using the real part of impedance perturbed by 2% random noise.

rectly. Figure 3b shows PG–corrected, physically realistic DRT, which consists of two peaks corresponding to the two RC–circuits. Peak positions on the frequency scale (0.0152 and 0.169 Hz) agree well with the characteristic frequencies $f = 1/(2\pi RC)$ of 0.0159 and 0.159 Hz, for $R = 5, C = 2$ and $R = C = 1$, respectively. The fractions of polarization resistivity resulted from DRT are 0.83893 and 0.16714; the ratio of these values is 5.02, which is in good agreement with the ratio of RC–circuit resistivities of 5.0. Note that unlike the exact Dirac delta–functions solution, the peaks in Figure 3b are wide; however, these peaks are located at correct places and they give correct polarization resistances. This is all that one may expect from DRT analysis.

The next test is the Warburg finite–length impedance

$$Z_W = \frac{\tanh\left(\sqrt{i\tau_*\omega}\right)}{\sqrt{i\tau_*\omega}} \qquad (17)$$

where τ_* is the characteristic time constant of the transport process. Setting $\tau_* = 1$ generating impedance (17) in the frequency range from 10^{-2} to 10^4 Hz on a grid with 22 points per decade, and calculating DRT according to the TRPG–scheme with the real part of impedance, we get a curve in Figure 4a. A feature of Warburg impedance is large spectral range covering nearly five decades. The leftmost peak located at 0.390 Hz exhibits the main transport process (Figure 4). It is easy to show that with $\tau_* = 1$, the exact position of $-\mathrm{Im}\,(Z_W)$ peak is at 0.404 Hz. Thus, the value of 0.390 Hz in Figure 4a is in good agreement with the exact result. It is worth noting a high–frequency peak at 731 Hz; this peak and the two shoulders going down to nearly 2 Hz represent the high–frequency straight line of the Warburg spectrum in the Nyquist coordinates. Similar wide peak manifesting proton transport in the cathode catalyst layer (CCL) is a characteristic feature of PEM fuel cell DRT spectrum (to be published elsewhere).

To demonstrate the effect of noise, the DRT of Warburg impedance is calculated using the real part of impedance perturbed by a 2% random noise (Figure 4b). As can be seen, the main transport peak is at the same position (0.390 Hz). Note that due to noise, a phantom peak appears at 1.37 Hz (Figure 4b); however, the contribution of of this peak to the polarization resistance is small.

The final, accurate values of the two regularization parameters are calculated by the method; the user should only set correct order–of–magnitude estimates for λ_T and λ_{pg} to start calculations. In the current version of the code, the choice of initial λ_T is performed using the L–curve method[35]; initial λ_{pg} is calculated from Eq.(15).

B. DRT of the cathode catalyst layer

One of the key problems in PEM fuel cell design is understanding the laws of oxygen transport in the cathode

View Article Online
DOI: 10.1039/D0CP02094J

catalyst layer. Of particular interest is unexpected over–linear transport loss due to oxygen transport in the Nafion film covering Pt/C agglomerates in low–Pt CCLs (see reviews[36,37]). Can DRT help to understand transport properties of the CCL? In this section, an attempt to approach the problem is done.

Analytical expression for impedance Z_{ctox} of the CCL with fast proton transport and finite rate of oxygen transport is[38]

$$Z_{ctox} = b\Bigg\{ \mathrm{i}\omega C_{dl} b l_t + \left(\tilde{R}_W + \mathrm{i}\frac{i_* \exp(\eta_0/b)}{4Fc_h^{in}\omega}\left(\tilde{R}_W - \tilde{Z}_W\right)\right) \times i_* l_t \left(\frac{c_1}{c_h^{in}}\right)\exp\left(\frac{\eta_0}{b}\right)\Bigg\}^{-1} \quad (18)$$

where

$$\tilde{Z}_W = \frac{\tanh\sqrt{\dfrac{i_* l_t^2 \exp(\eta_0/b)}{4FD_{ox}c_h^{in}} + \mathrm{i}\dfrac{l_t^2\omega}{D_{ox}}}}{\sqrt{\dfrac{i_* l_t^2 \exp(\eta_0/b)}{4FD_{ox}c_h^{in}} + \mathrm{i}\dfrac{l_t^2\omega}{D_{ox}}}}, \qquad \tilde{R}_W = \tilde{Z}_W\Big|_{\omega=0} \quad (19)$$

Here, b is the oxygen reduction reaction (ORR) Tafel slope, C_{dl} is the double layer volumetric capacitance (F cm^{-3}), l_t is the CCL thickness, η_0 is the total oxygen reduction reaction (ORR) overpotential, positive by convention, c_h^{in} is the reference (inlet) oxygen concentration, c_1 is the oxygen concentration at the CCL/gas–diffusion layer interface, D_{ox} is the oxygen diffusion coefficient in the CCL, and i_* is the ORR exchange current density.

Eq.(18) includes faradaic (charge–transfer) and oxygen transport impedances. In case of fast proton transport, the ORR overpotential η_0 and cell current density j_0 are related by the following polarization curve[39]

$$\tilde{j}_0 = \tilde{D}_{ox}\sqrt{\frac{\exp\tilde{\eta}_0}{\tilde{D}_{ox}}}\tanh\sqrt{\frac{\exp\tilde{\eta}_0}{\tilde{D}_{ox}}} \quad (20)$$

where tilde marks the dimensionless variables:

$$\tilde{j}_0 \quad \frac{j_0}{i_* l_t}, \quad \tilde{\eta}_0 \quad \frac{\eta_0}{b}, \quad \tilde{D}_{ox} \quad \frac{4FD_{ox}c_h^{in}}{i_* l_t^2} \quad (21)$$

Eq.(18) works if the cell current density j_0 satisfies to

$$j_0 \ll \frac{\sigma_p b}{l_t} \quad (22)$$

where σ_p is the CCL proton conductivity. Eq.(22) means that j_0 must be sufficiently small to neglect variation of the ORR overpotential through the catalyst layer depth due to finite σ_p. For typical PEMFC parameters, Eq.(22) holds if the cell current density is below 100 mA cm^{-2}.

ORR Tafel slope b, V	0.03
ORR exchange current density i_*, A cm^{-3}	10^{-3}
Double layer capacitance C_{dl}, F cm^{-3}	10
Catalyst layer thickness l_t, cm	0.001
Cell temperature T, K	273 + 80
Air pressure p, bar	1.0
Reference oxygen concentration c_h^{in}, mol cm^{-3}	$7.155 \cdot 10^{-6}$
Cell current density j_0, A cm^{-2}	0.1

TABLE I. Parameters used in calculations. For simplicity we set $c_1 = c_h^{in}$.

Eq.(18) makes it possible to study the effect of CCL oxygen transport parameter on the DRT spectrum. Sixty six equidistant on the log–scale frequency points and the respective values of CCL impedance (18) have been generated in the frequency range from 1 to 10^3 Hz. The imaginary part of impedance $\mathrm{Im}\,(Z_{ctox})$ has been used to calculate DRT spectra. The results for the effective oxygen diffusion coefficient D_{ox} varying from $8\cdot10^{-5}$ cm^2 s^{-1} down to $5\cdot10^{-6}$ cm^2 s^{-1} are shown in Figure 5. The upper value of $8\cdot10^{-5}$ cm^2 s^{-1} is typical for standard "healthy" Pt/C–based cathodes[40], while the lower value of $5\cdot10^{-6}$ cm^2 s^{-1} is characteristic of flooded CCL.

Position of the right peak in Figures 5 does not change upon variation of D_{ox} and hence we can safely attribute this peak to faradaic process. The characteristic frequency f_{ct} of charge–transfer process in PEMFC is[41]

$$f_{ct} = \frac{j_0}{2\pi b C_{dl} l_t}. \quad (23)$$

With the parameters from Table I we get $f_{ct} \simeq 53.1$ Hz, which is in good agreement with the right peak position at $\simeq 60$ Hz in Figures 5a–e. Since the ORR Tafel slope and the CCL thickness are usually known, DRT spectrum and Eq.(23) allow us to estimate the double layer capacitance C_{dl} in the catalyst layer. Note that this estimate is only possible if the cell current is small; for large currents, Eq.(23) is not valid.

Evidently, the left DRT peak in Figures 5 is due to oxygen transport. If the oxygen transport losses in the CCL are small, position of this peak f_{ox} on the frequency scale is described by[42]

$$f_{ox} = \frac{2.54D_{ox}}{2\pi l_t^2} + \frac{j_0}{2\pi 4Fc_1 l_t}. \quad (24)$$

With the data from Table I, for $D_{ox} = 8\cdot10^{-5}$ cm^2 s^{-1} (Figure 5a), we get $f_{ox} \simeq 38$ Hz, which is close to the right side of the oxygen transport "shoulder" ($\simeq 30$ Hz) in this Figure. However, for D_{ox} $4\cdot10^{-5}$ cm^2 s^{-1} (Figure 5b), Eq.(24) gives $f_{ox} \simeq 22$ Hz, while the left peak in Figure 5b takes position at 14 Hz. The reason for this discrepancy is that with $D_{ox} = 4\cdot10^{-5}$ cm^2 s^{-1}, the oxygen transport loss

View Article Online
DOI: 10.1039/D0CP02094J 6

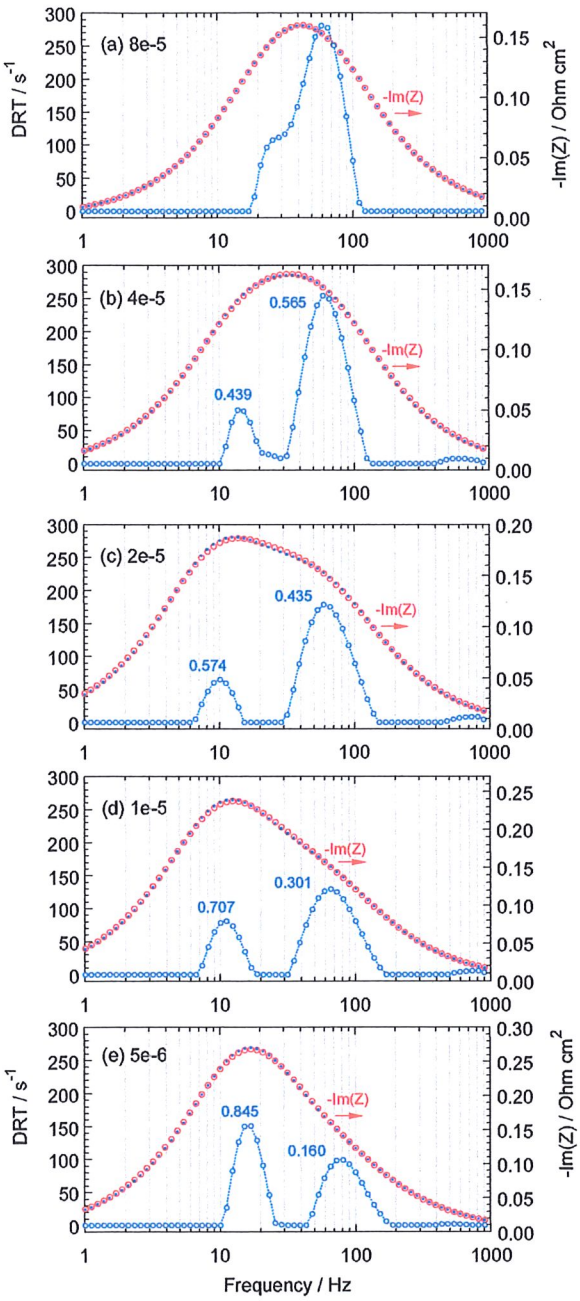

FIG. 5. Open circles – DRT of impedance of the PEMFC cathode catalyst layer with fast proton transport, Eq.(18). Indicated are the values of oxygen diffusion coefficient in the CCL D_{ox}, cm^2 s^{-1} (upper left corner). Numbers at the peaks show the fraction of the respective process in the total cell polarization resistance. Blue solid points – calculated using Eq.(18) imaginary part of the CCL impedance Im (Z_{ctox}), red open circles – Im (Z_{ctox}) reconstructed from DRT.

is not small, and Eq.(24) overestimates f_{ox}. The oxygen transport loss is small, if the cell current density is much less than the characteristic current density j_{ox} for oxygen transport in the CCL[39]

$$j_0 \ll j_{ox} = \frac{4FD_{ox}c_1}{l_t} \tag{25}$$

With the parameters in Table I and $D_{ox} = 4\cdot10^{-5}$ cm^2 s^{-1} we find $j_{ox} = 0.11$ A cm^{-2}, meaning that $j_0 \simeq j_{ox}$ and Eq.(24) is not valid. Nonetheless, qualitatively, as D_{ox} decreases down to $D_{ox} = 2\cdot10^{-5}$ cm^2 s^{-1}, the transport peak continues moving to lower frequencies (Figure 5c).

However, with the further decrease of D_{ox} the oxygen transport peak starts moving back, toward higher frequencies (Figures 5e,d). The range of D_{ox} below 10^{-5} cm^2 s^{-1} corresponds to severely flooded CCL. Thus, in accelerated stress testing experiments, the reverse motion of the oxygen transport peak may serve as indicator of significant worsening of the layer oxygen transport properties.

Finally, it is worth noting that the contribution of oxygen transport to the cell polarization resistance monotonically increases with the decrease in D_{ox} (see numbers at peaks in Figure 5). This is a quite expected result. If the oxygen transport loss is small, the equation for CCL oxygen transport resistance[10]

$$R_{ox} = \frac{bl_t}{12FD_{ox}c_1} \tag{26}$$

allows one to estimate D_{ox} from the DRT data.

IV. CONCLUSIONS

A simple and fast method for calculation of distribution of relaxation times for PEM fuel cell impedance is reported. The method combines Tikhonov regularization technique with projected gradient method. The optimal values of two regularization parameters are found using least–squares minimization of the Tikhonov residual.

The method is tested using synthetic impedance of two series–connected RC–circuits and Warburg finite–length impedance. The method is applied to derive DRT of analytical impedance of the PEMFC cathode catalyst layer with fast proton transport. Decrease of the oxygen diffusion coefficient D_{ox} in the CCL leads to non–monotonic movement of the oxygen transport peak along the frequency axis. For D_{ox} below 10^{-5} cm^2 s^{-1}, the peak moves toward higher frequencies as Dox decreases. This effect can serve as indicator of cathode flooding. The advantages of TRPG method suggested in this work are simplicity, fast speed, and availability as open–source Python code at https://github.com/akulikovsky/DRT-python-code .

View Article Online
DOI: 10.1039/D0CP02094J 7

APPENDIX. G–FUNCTION VERSION OF THE METHOD

Eq.(1) can be written in equivalent form as

$$Z(\omega) - R_\infty = R_{pol} \int_{-\infty}^{+\infty} \frac{G(\tau)\, d\ln(\tau)}{1 + i\omega\tau} \qquad (27)$$

where $G(\tau) = \tau\gamma(\tau)$. Numerical approximation for imaginary part of Eq.(27) is $\mathbf{A}\vec{G} = \vec{Z}''$ where the matrix $A_{m,n}$ is

$$A_{m,n} = -R_{pol} \frac{\omega_m \tau_n \delta\ln(\tau_n)}{1 + \omega_m^2 \tau_n^2}; \qquad \delta\ln(\tau_n) = \ln(\tau_{n+1}) - \ln(\tau_n) \qquad (28)$$

The rest part of the algorithm is described by Eqs.(9)–(11) with the evident replacement γ by G. Note that in Eq.(27), the mesh step $\delta\ln(\tau_n)$ is usually independent of n, as experimental impedance is typically measured on equidistant log–scale grid.

In this variant, the method returns function $G(\tau)$, which is used in most of the works on DRT analysis. On the frequency scale, the following relation holds

$$G(f) = \frac{\gamma(f)}{2\pi f} \qquad (29)$$

meaning that the high–frequency peaks of $G(f)$ are dumped and the low–frequency peaks are enhanced as compared to the respective peaks in $\gamma(f)$–spectrum. Note that Eq.(29) shifts position of peaks on the frequency scale, as the high–frequency wing of the $\gamma(f)$ peak is divided by larger f as compared to the low–frequency wing. Correct comparison of peak positions with the characteristic frequencies of the physical processes should be done using $\gamma(f)$. For example, in the test with two RC–circuits (Figure 3), the right peak of $G(f)$ appears at 0.183 Hz, while the correct position of $\gamma(f)$ peak is 0.159 Hz. As an example, Warburg finite–length DRT spectrum in terms of $G(f)$ calculated as discussed in this section is shown in Figure 6.

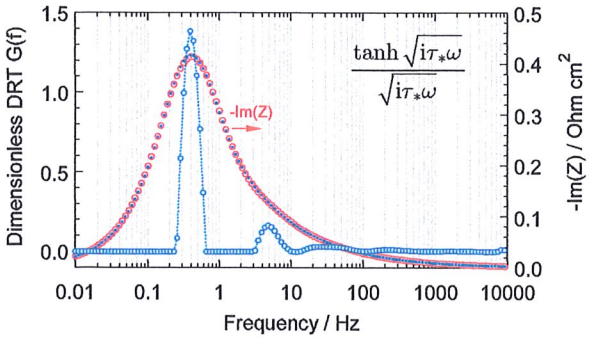

FIG. 6. DRT $G(f)$, Eq.(27) of Warburg finite–length impedance, Eq.(17) (connected blue open circles) calculated using the TRPG–scheme described in Appendix. Solid blue points depict imaginary part of exact impedance, Eq.(17), open red circles show $-\mathrm{Im}\,(Z)$ reconstructed from the DRT.

CONFLICT OF INTEREST STATEMENT

The author declares no conflict of interest.

[1] M. E. Orazem and B. Tribollet, *Electrochemical Impedance Spectroscopy*, Wiley, New–York, 2008.
[2] A. Lasia, *Electrochemical Impedance Spectroscopy and its Applications*, Springer, New York, 2014.
[3] A. Kulikovsky, *Analytical Models for PEM Fuel Cell Impedance*, Self–publishing, Eisma, 2018.
[4] S. Arisetty, X. Wang, R. K. Ahluwalia, R. Mukundan, R. Borup, J. Davey, D. Langlois, F. Gambini, O. Polevaya and S. Blanchet, *J. Electrochem. Soc.*, 2012, **159**, B455–B462.
[5] M. S. Kondratenko, M. O. Gallyamov and A. R. Khokhlov, *Int. J. Hydrogen Energy*, 2012, **37**, 2596 – 2602.
[6] A. C. Okafor and H.-M. C. Mogbo, *J. Fuel Cell Sci. Techn.*, 2012, **9**, 011006–1–011006–13.
[7] J. Kim, J. Lee and B. H. Cho, *IEEE Trans. Ind. Electronics*, 2013, **60**, 5086–5094.
[8] I. A. Schneider, M. H. Bayer and S. von Dahlen, *J. Electrochem. Soc.*, 2011, **158**, B343–B348.
[9] J. Mainka, G. Maranzana, A. Thomas, J. Dillet, S. Didierjean and O. Lottin, *Fuel Cells*, 2012, **12**, 848–861.
[10] A. A. Kulikovsky, *J. Electrochem. Soc.*, 2015, **162**, F217–F222.
[11] A. Baricci and A. Casalegno, *Electrochim. Acta*, 2015, **157**, 324–332.
[12] D. Gerteisen, *J. Electrochem. Soc.*, 2015, **162**, F1431–F1438.
[13] B. P. Setzler and T. F. Fuller, *J. Electrochem. Soc.*, 2015, **162**, F519–F530.
[14] C. Bao and W. G. Bessler, *J. Power Sources*, 2015, **278**, 675–682.
[15] T. Reshetenko and A. Kulikovsky, *J. Electrochem. Soc.*, 2018, **165**, F291–F296.
[16] T. Reshetenko and A. Kulikovsky, *RSC Adv.*, 2019, **9**, 38797–38806.
[17] H. Schichlein, A. C. Müller, M. Voigts, A. Krügel and E. Ivers-Tiffée, *J. Appl. Electrochem.*, 2002, **32**, 875–882.
[18] A. B. Tesler, D. R. Lewin, S. Baltianski and Y. Tsur, *J. Electroceram.*, 2010, **24**, 245–260.
[19] D. Klotz, J. P. Schmidt, A. Kromp, A. Weber and E. Ivers-Tiffée, *ECS Trans.*, 2012, **41**, 25–33.
[20] Y. Zhang, Y. Chen, M. Yan and F. Chen, *J. Power Sources*, 2015, **283**, 464–477.
[21] B. A. Boukamp, *Electrochim. Acta*, 2017, **252**, 154–163.
[22] M. Heinzmann, A. Weber and E. Ivers-Tiffée, *J. Power Sources*, 2019, **444**, 227279.
[23] R. Fuoss and J. Kirkwood, *J. Am. Chem. Soc.*, 1941, **63**, 385–394.
[24] E. Ivers-Tiffée and A. Weber, *J. Ceramic Soc. Japan*, 2017, **125**, 193–201.
[25] A. A. Kulikovsky, *J. Electroanal. Chem.*, 2014, **738**, 108–112.
[26] A. N. Tikhonov and V. Y. Arsenin, *Solutions of Ill–Posed Problems*, Wiley, New–York, 1977.
[27] J. Macutkevic, J. Banys and A. Matulis, *Nonlin. Analysis: Modelling and Control*, 2004, **9**, 75–88.
[28] P. Büschel, U. Tröltzsch and O. Kanoun, 9th International Multi-Conference on Systems, Signals and Devices (SSD), 2012, pp. 1–3.
[29] M. Saccoccio, T. H. Wan, C. Chen and C. F, *Electrochim. Acta*, 2014, **147**, 470–482.
[30] T. H. Wan, M. Saccoccio, C. Chen and F. Ciucci, *Electrochim. Acta*, 2015, **184**, 483–499.
[31] M. Heinzmann, A. Weber and E. Ivers-Tiffée, *J. Power Sources*, 2018, **402**, 24 – 33.
[32] B. A. Boukamp, *Electrochim. Acta*, 2015, **154**, 35–46.
[33] S. Hershkovitz, S. Tomer, S. Baltianski and Y. Tsur, *ECS Trans.*, 2011, **33**, 67–73.
[34] A. N. Iusem, *Comput. Appl. Math.*, 2003, **22**, 37–52.

View Article Online
DOI: 10.1039/D0CP02094J 8

[35]T. M. Correia, A. P. Gibson, M. Schweiger and J. C. Hebden, *J. Biomed. Optics*, 2009, **14**, 1–11.
[36]A. Kongkanand, W. Gu and M. Mathias, *Fuel Cells and Hydrogen production*, Springer, New–York, 2018, pp. 323–342.
[37]A. Kusoglu, *Fuel Cells and Hydrogen production*, Springer, New–York, 2018, pp. 417–438.
[38]A. A. Kulikovsky, *Electrochim. Acta*, 2016, **225**, 559–565.
[39]A. A. Kulikovsky, *Electrochim. Acta*, 2010, **55**, 6391–6401.
[40]T. Reshetenko and A. Kulikovsky, *J. Electrochem. Soc.*, 2016, **163**, F1100–F1106.
[41]A. A. Kulikovsky and M. Eikerling, *J. Electroanal. Chem.*, 2013, **691**, 13–17.
[42]A. A. Kulikovsky, *Electrochim. Acta*, 2016, **196**, 231–235.

NOMENCLATURE

~	Marks dimensionless variables
b	ORR Tafel slope, V
C_{dl}	Double layer volumetric capacitance, F cm^{-3}
c_1	Oxygen molar concentration at the CCL/GDL interface, mol cm ^{3}
c_h^{in}	Reference (inlet) oxygen concentration, mol cm^{-3}
D_{ox}	Oxygen diffusion coefficient in the CCl, cm^2 s^{-1}
F	Faraday constant, C mol^{-1}
f_{ct}	Characteristic frequency of faradaic process, Hz
f_{ox}	Characteristic frequency of oxygen transport in the CCL, Hz
G	G–function DRT, Eq.(29)
i_*	ORR volumetric exchange current density, A cm^{-3}
i	Imaginary unit
j_{ox}	Limiting current density due to oxygen transport in the CCL, A cm^{-2}
j_p	Limiting current density due to proton transport in the CCL, A cm^{-2}
j_0	Cell current density, A cm^{-2}
l_t	CCL thickness, cm
R_{pol}	Cell polarization resistance, Ω cm^2
R_∞	High frequency (ohmic) resistance, Ω cm^2
Z	Cell impedance Ω cm^2

Subscripts:

0 Membrane/CCL interface
1 CCL/GDL interface

Greek:

γ	DRT, s^{-1}
η_0	ORR overpotential, positive by convention, V
σ_p	Catalyst layer proton conductivity, Ω^{-1} cm^{-1}
τ	Time constants scale ($\tau = 1/\omega$), s
ω	Angular frequency of the AC signal, s^{-1}